

Raman spectra of barium halides in orthorhombic and hexagonal symmetry: An *ab initio* studyChristian Bohley,^{1,*} Jan-Martin Wagner,^{2,3} Charlotte Pfau,¹ Paul-Tiberiu Miclea,^{4,5} and Stefan Schweizer^{1,4}¹*Centre for Innovation Competence SiLi-nano[®], Martin Luther University of Halle-Wittenberg, Karl-Freiherr-von-Fritsch-Str. 3, DE-06120 Halle (Saale), Germany*²*Max Planck Institute of Microstructure Physics, Weinberg 2, DE-06120 Halle (Saale), Germany*³*Institute for Materials Science, Christian-Albrechts-University at Kiel, Kaiserstr. 2, DE-24143 Kiel, Germany*⁴*Fraunhofer Center for Silicon Photovoltaics, Walter-Hülse-Str. 1, DE-06120 Halle (Saale), Germany*⁵*Institute of Physics, Martin Luther University of Halle-Wittenberg, Heinrich-Damerow-Str. 4, DE-06120 Halle (Saale), Germany*

(Received 28 September 2010; published 28 January 2011; corrected 14 February 2011)

Vibrational properties of bulk crystalline barium halides BaCl₂, BaBr₂, and BaI₂ are theoretically investigated for orthorhombic and hexagonal symmetry with *ab initio* methods in density functional theory. It is demonstrated that the used method is capable of predicting frequencies of vibrational modes, their symmetry types, and corresponding Raman intensities in reasonable agreement with experimental data for orthorhombic and hexagonal BaCl₂ and BaBr₂ nanocrystals embedded in fluorozirconate glasses. For orthorhombic BaCl₂, a Raman-active phonon mode could be predicted theoretically that was not observed in measurements before.

DOI: [10.1103/PhysRevB.83.024107](https://doi.org/10.1103/PhysRevB.83.024107)

PACS number(s): 78.30.-j, 63.20.dk, 63.50.-x, 77.22.Ch

I. INTRODUCTION

The vibrational energies of the barium halides BaCl₂, BaBr₂, and BaI₂ in orthorhombic and hexagonal symmetry are, apart from theoretical interest, critical for fluorescence applications of these materials when embedded as nanocrystals in glasses. Fluorescent fluorozirconate glasses containing rare earth (RE) activated barium halide nanocrystals have great potential for use as x-ray storage phosphors or scintillators for medical imaging.^{1,2} They are also attractive for further applications such as up- or down-conversion layers for high efficiency solar cells.^{3,4} For high fluorescence efficiencies nonradiative losses in the RE host material can be reduced by using host materials with low phonon energies, e.g., fluorozirconate (FZ) glasses (< 590 cm⁻¹).^{5,6} If these glasses are additionally doped with Cl or Br ions the growth of nanocrystals during a subsequent annealing procedure is initiated. The BaCl₂ and BaBr₂ nanocrystals are appropriate hosts for the RE ions and improve the fluorescence efficiency of these systems further because of the very low maximum phonon energies.

Experimentally, Raman spectra of orthorhombic BaCl₂ and BaBr₂ were investigated in the 1970s by Sadoc *et al.*⁷ and Monberg *et al.*,⁸ respectively. Raman spectra of those barium halides are uncommon in literature because of the high hygroscopicity of these compounds. Raman spectra of hexagonal and orthorhombic BaCl₂ and BaBr₂ nanocrystals were measured recently by Pfau *et al.*⁶ So far, vibrational properties of hexagonal bulk crystals of BaCl₂, BaBr₂, and BaI₂, as well as the orthorhombic BaI₂, have not been determined because of their thermodynamic instability.^{9,10} Theoretical considerations about phonons of barium halides were outlined until recently only for BaF₂ in the simpler cubic symmetry *Fm* $\bar{3}$ *m*.^{11,12} The stability of an unobserved crystalline BaCl compound in rocksalt structure was predicted in Ref. 13 based on elasticity and phonon properties obtained from the density functional theory (DFT).

Here, the Raman spectra of bulk BaCl₂, BaBr₂, and BaI₂ in orthorhombic and hexagonal symmetry (see the stereo

sketches¹⁴ in Fig. 1) are studied theoretically and for the first two, are compared with Raman measurements of bulk crystals^{7,8} and of nanocrystals in fluorozirconate glasses.⁶ The symmetry-adapted types of the calculated modes are identified and the phonon bands in the measured Raman spectra are assigned to their symmetry modes.

II. METHODS

First-principle calculations within local density approximation (LDA) to density functional theory were performed in order to determine the phonon frequencies and the corresponding Raman scattering intensities of bulk crystalline BaCl₂, BaBr₂, and BaI₂ in orthorhombic and hexagonal symmetry. The implementation in the ABINIT package^{15,16} was used with the Teter extended norm-conserving pseudopotential for Ba (Ref. 17) and pseudopotentials for the halides Cl, Br, and I in the Troullier-Martins pseudopotential scheme.¹⁸ For Ba, the 5*s*, 5*p*, and 6*s* electrons, and for the halides those of the *s* and *p* orbitals of the outermost shell were treated as valence electrons.

The kinetic cutoff energies (ecut) for the plane-wave basis in reciprocal space and the number of bands (nband) for which wave functions were computed are given in Table I. These values were obtained from evaluating convergence tests after optimization of the atomic positions in the unit cell. For the replacement of integrals over the Brillouin zone, a 6 × 6 × 6 Monkhorst grid¹⁹ for the orthorhombic structures and a 4 × 4 × 4 Monkhorst grid for the hexagonal lattices were sufficient for the convergence of the variables required for phonon calculations.

The dynamical matrix that yields the phonon frequencies and eigendisplacements was computed within the variational approach of density functional perturbation theory. Following group theory, the dynamical matrix can be decomposed into blocks that correspond to an irreducible representation of the dynamical matrix group. This representation gives the infrared and Raman-active modes of the crystal structure. Nonresonant Raman scattering is a Stokes process initialized

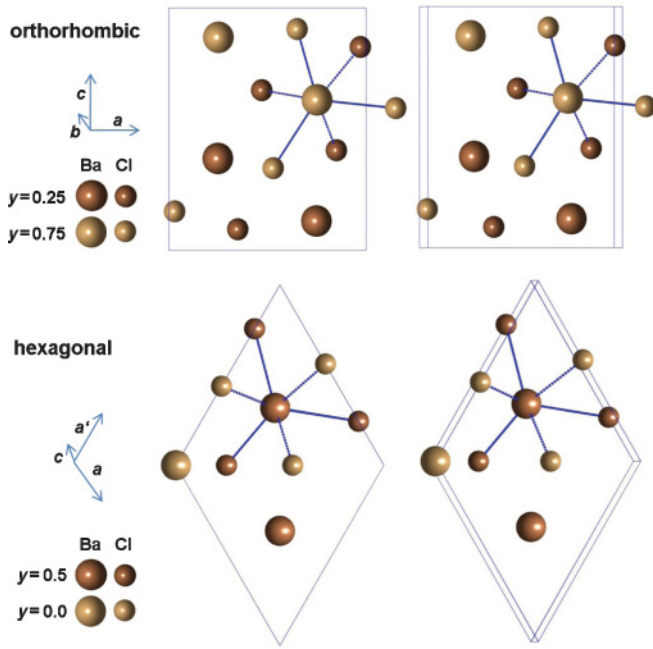


FIG. 1. (Color online) Stereo view of atom positions and unit cells of BaCl_2 in orthorhombic (top) and hexagonal symmetry (bottom) (after Table I). The y numbers in the legends are the altitudes in the projection plane. Connecting bond lines between Ba and Cl atoms are added in order to emphasize the similarity of both structures.

by an incoming photon with frequency ω_0 and polarization \mathbf{e}_0 . In the crystal lattice, this photon creates a phonon of frequency ω_m and is scattered to a photon with frequency $(\omega_0 - \omega_m)$ and polarization \mathbf{e}_s . The efficiency of this Raman scattering can be computed from the projection of the Raman susceptibility tensors on the polarization vectors \mathbf{e}_s and \mathbf{e}_0 . The form of the Raman susceptibility tensors depends on the phonon mode. The scattering intensity of a specific phonon mode m is determined by the specific Raman-scattering efficiency S with

$$\frac{dS}{d\Omega} = \frac{(\omega_0 - \omega_m)^4}{c^4} |\mathbf{e}_s \cdot \alpha_m \cdot \mathbf{e}_0|^2 \frac{\hbar}{2\omega_m} (n_m + 1), \quad (1)$$

where Ω is the collection angle of the scattered photon, c is the light velocity, \hbar is the reduced Planck constant, and α_m is the Raman tensor. The latter depends on variations of the linear electronic dielectric susceptibility tensor along atomic displacements described by the phonon eigendisplacement vector. The dependency of S on the temperature T is given by the factor

$$n_m = \frac{1}{\exp(\hbar\omega_m/k_B T) - 1}, \quad (2)$$

which includes again the phonon frequency ω_m , k_B being the Boltzmann constant. The Raman tensor and the frequency of a phonon mode can be numerically evaluated with the ABINIT code. More details can be found in Refs. 16 and 22. For comparison with experimental data, the Raman intensities were calculated as an average over all possible crystal orientations and over all polarizations as it is useful for powder spectra; for the applied formulas, see Refs. 16 and 23.

TABLE I. Computational and structural parameters used in the DFT studies of the phonon response of bulk orthorhombic and hexagonal BaCl_2 , BaBr_2 , and BaI_2 . Cell size and atom parameters are obtained with structural relaxation performed with ABINIT. For comparison, experimental values of cell size and atomic parameters are given in parentheses, taken for BaCl_2 and BaBr_2 from Ref. 20, for BaI_2 in orthorhombic symmetry from Ref. 21, and in hexagonal symmetry from Ref. 9.

$Pnma$	BaCl_2	BaBr_2	BaI_2
ecut/Ha	70	75	75
nband	50	50	52
$a/\text{\AA}$	7.72 (7.88)	8.10 (8.28)	8.72 (8.92)
$b/\text{\AA}$	4.66 (4.73)	4.84 (4.96)	5.18 (5.30)
$c/\text{\AA}$	9.26 (9.44)	9.69 (9.92)	10.45 (10.7)
x_{Ba}	0.248 (0.251)	0.249 (0.245)	0.248 (0.237)
z_{Ba}	0.116 (0.121)	0.119 (0.115)	0.119 (0.121)
$x_{\text{ha},1}$	0.142 (0.150)	0.140 (0.142)	0.141 (0.139)
$z_{\text{ha},1}$	0.429 (0.413)	0.428 (0.427)	0.427 (0.427)
$x_{\text{ha},2}$	0.026 (0.029)	0.026 (0.028)	0.025 (0.029)
$z_{\text{ha},2}$	0.830 (0.839)	0.831 (0.840)	0.833 (0.839)
$P\bar{6}2m$	BaCl_2	BaBr_2	BaI_2
ecut/Ha	80	95	85
nband	48	48	46
$a/\text{\AA}$	7.88 (8.11)	8.25 (8.48)	8.94 (9.15)
$c/\text{\AA}$	4.54 (4.65)	4.77 (4.82)	5.05 (5.17)
$x_{\text{ha},1}$	0.256 (—)	0.256 (—)	0.256 (0.256)
$x_{\text{ha},2}$	0.589 (—)	0.590 (—)	0.594 (0.592)

This method gives no information on the shape or the width of the Raman intensity scattered by a single mode because electron-phonon coupling has not been taken into account. For the calculated spectra shown in Figs. 2–4, Raman peaks are assumed to be of Lorentzian shape with a small full width half maximum linewidth of 2 cm^{-1} . Using a larger linewidth of 8 cm^{-1} provides a good qualitative agreement of the calculated spectra with the measured spectra by Pfauf *et al.*⁶

The measurements taken from Ref. 6 were performed with barium halide nanocrystals in glasses based on the ZBLAN ($53\text{ZrF}_3\text{-}20\text{BaF}_2\text{-}20\text{NaF-}4\text{LaF}_3\text{-}3\text{AlF}_3$, values are in mol%) composition.²⁴ The fluorochlorozirconate (FCZ) and fluorobromozirconate (FBZ) glasses consist basically of a mixture of zirconium, barium, and sodium fluorides to which barium and sodium chlorides and bromides, respectively, are added. The preparation method is described in Refs. 6 and 25. To initiate the formation of orthorhombic and hexagonal barium halide nanocrystals the FCZ and FBZ glasses were subsequently treated at different appropriate annealing conditions. The achieved content of BaCl_2 and BaBr_2 crystallites is at most 20 and 7.5 mol%, respectively, assuming complete crystallization. Unpolarized Raman measurements were done in reflection geometry. For the excitation the 514.5 nm line of an argon ion laser was used.

III. RESULTS

Here, BaCl_2 , BaBr_2 , and BaI_2 in orthorhombic $Pnma$ (space group 62, in Schoenflies notation D_{2h}^{16}) and hexagonal $P\bar{6}2m$ (space group 189, D_{3h}^3) symmetries are considered. The

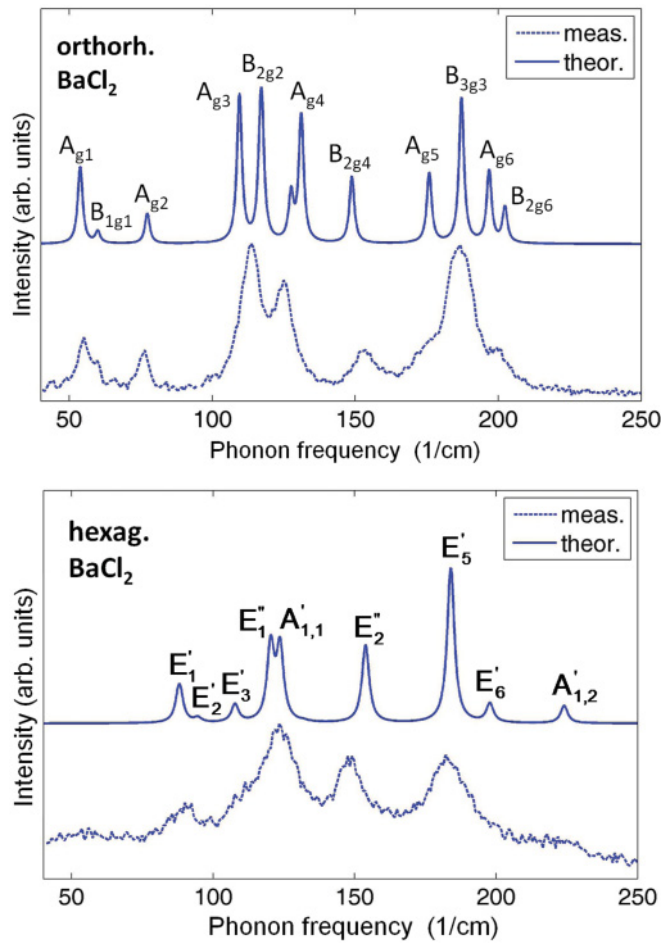


FIG. 2. (Color online) Comparison of Raman spectra of orthorhombic (top) and hexagonal (bottom) BaCl_2 obtained from the DFT to the measured Raman intensity of corresponding nanocrystals in an FCZ glass.⁶ The dominant peaks are assigned to their symmetry modes.

orthorhombic cell contains four formula units, i.e., four Ba and eight halide atoms, and the hexagonal cell contains three formula units, i.e., three Ba and six halide atoms (see Fig. 1). Each Ba^{2+} ion has nine halide ion neighbors, three lying in the same plane that was used as the projection plane in Fig. 1, three lying in a plane behind, and three lying in a plane in front of that plane.

In the orthorhombic unit cell, two Ba and two inequivalent halide atoms occupy Wyckoff $4c$ positions, respectively, while in the hexagonal unit cell, two inequivalent Ba atoms occupy the Wyckoff $1b$ and $2c$ positions and the inequivalent halide atoms occupy the Wyckoff $3f$ and $3g$ positions, respectively.

The cell size parameters used for the DFT calculations are obtained with structural relaxation performed with ABINIT. The values x_{Ba} , z_{Ba} , $x_{\text{ha},1}$, $z_{\text{ha},1}$, $x_{\text{ha},2}$, and $z_{\text{ha},2}$ are the structural parameters of the barium and the halide ions at the $4c$ Wyckoff positions in the unit cell of the orthorhombic $Pnma$ structure, respectively. The calculated structural parameters $x_{\text{ha},1}$ and $x_{\text{ha},2}$ (see Table I) for the $3f$ and $3g$ Wyckoff positions for the hexagonal BaCl_2 , BaBr_2 , and BaI_2 are very close to their experimental counterparts, e.g., $x_{\text{ha},1} = 0.2563$ and $x_{\text{ha},2} = 0.5918$ determined by Beck⁹ for hexagonal BaI_2 with x-ray diffraction.

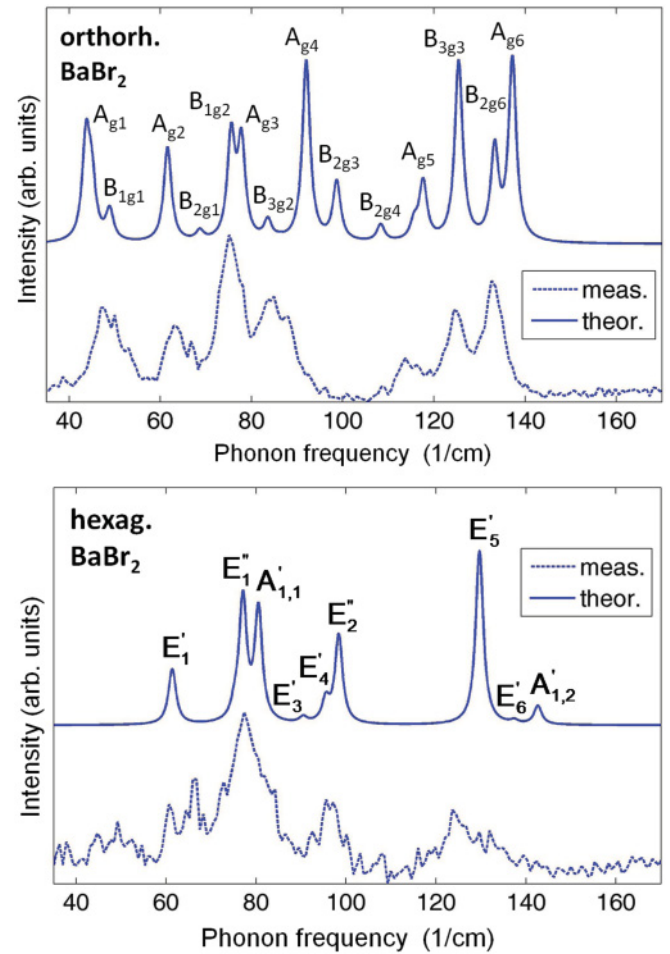


FIG. 3. (Color online) Comparison of Raman spectra of orthorhombic (top) and hexagonal (bottom) BaBr_2 obtained from DFT to the measured Raman intensity of corresponding nanocrystals in an FBZ glass.⁶ The dominant peaks are assigned to their symmetry modes.

At the zone center three acoustic and 33 optical phonon modes are expected for the orthorhombic crystal and three acoustic and 24 optical phonon modes for the hexagonal crystal. Factorial group analysis predicts for the orthorhombic $Pnma$ symmetry 18 Raman-active modes ($6A_g + 3B_{1g} + 6B_{2g} + 3B_{3g}$), where every Wyckoff $4c$ position corresponds to one A_g , two B_{1g} , one B_{2g} , and two B_{3g} modes, 12 infrared-active modes ($5B_{1u} + 2B_{2u} + 5B_{3u}$) and three silent modes ($3A_u$). The hexagonal crystal has ten Raman-active modes ($2A'_1 + 6E' + 2E''$), nine infrared-active modes ($3A''_1 + 6E'$), and three silent modes ($2A'_2$ and $1A''_1$). The E' modes are both infrared and Raman active. Here, the notation of Loudon²⁶ was used.

A nonstandard choice of the coordinate axes can cause confusion regarding the vibration mode assignment for crystals of the same space group. In Ref. 8 (see also the comparison in Table II) the 18 measured Raman modes of orthorhombic BaBr_2 are assigned to $6A_g + 6B_{1g} + 3B_{2g} + 3B_{3g}$ because the axis system was chosen after Wyckoff²⁷ with the crystal in orthorhombic $Pbnm$ symmetry. Today's standard follows the *International Tables for Crystallography*²⁸ describing the orthorhombic BaCl_2 and BaBr_2 in $Pnma$ symmetry

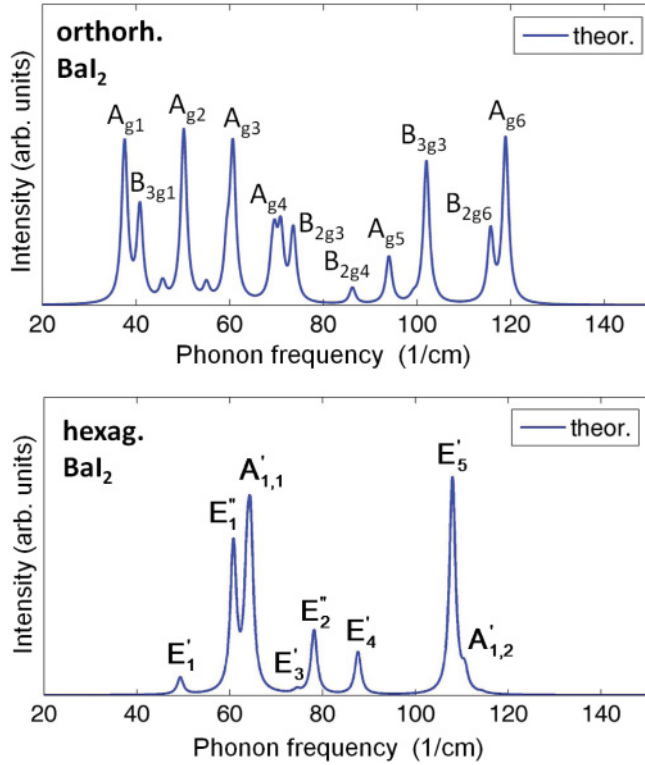


FIG. 4. (Color online) Raman spectra of orthorhombic (top) and hexagonal (bottom) BaI_2 obtained from DFT. The dominant peaks are assigned to their symmetry modes.

of the prototype PbCl_2 (see also remarks in Ref. 29). The three B_{3g} modes in $Pbnm$ symmetry detected by Monberg are understood here as B_{1g} modes in $Pnma$ symmetry, the six B_{1g} modes in $Pbnm$ symmetry are understood as B_{2g} modes in $Pnma$ symmetry, and the three B_{2g} modes in $Pbnm$ symmetry are understood as B_{3g} modes in $Pnma$ symmetry. The first and second B_{1g} mode in Ref. 8 (here, B_{2g}) at 48 cm^{-1} and 53 cm^{-1} , respectively, and the third B_{2g} mode in Ref. 8 (here, B_{3g}) at 136 cm^{-1} could not be assigned to the modes obtained from the DFT calculations. Possibly, these modes were misinterpreted in Ref. 8 because of spillover effects from orientations that reveal other modes. For instance, the peak at 136 cm^{-1} , interpreted as the third B_{2g} mode in $Pbnm$ symmetry in Ref. 8, could be effectively the sixth A_g mode, measured at 134 cm^{-1} , whereas the first B_{3g} mode at 45 cm^{-1} predicted with the theory could be overlooked because of a very low intensity.

For BaCl_2 and BaBr_2 in orthorhombic and hexagonal symmetry, the predicted Raman frequencies and intensities correspond well to the data extracted from the measured Raman spectra from Ref. 6 shown in Figs. 2 and 3. These spectra are phonon responses from nanocrystals in glass and therefore, phonon peaks are broader than peaks measured in bulk crystals. Apart from quantum confinement effects, this can be caused by a broad size distribution of the nanocrystals and disorder effects such as poor crystalline quality or shape irregularities.³⁰ As reported in Ref. 6, a measurable shift of the phonon frequencies of the nanocrystals compared to the corresponding frequencies in bulk crystal was not observed.

In a rough estimate following the model of vibrations of a chain of atoms of two types, one would expect the optical

TABLE II. Calculated wave numbers (values in cm^{-1}) of the Raman-active zone-center phonon modes in orthorhombic $Pnma$ BaCl_2 , BaBr_2 , and BaI_2 and the assignments to their symmetry-adapted types. For comparison the BaCl_2 modes measured by Sadoc *et al.*⁷ and Pfau *et al.*,⁶ and the BaBr_2 modes measured by Monberg *et al.*⁸ and Pfau *et al.*⁶ are given in parentheses (see the text). No Raman measurements were available for BaI_2 .

A_g	B_{1g}	B_{2g}	B_{3g}
BaCl_2 $Pnma$			
54 (57,55)	60 (61,60)	95 (98, —)	54 (57,55)
77 (77,76)	117 (112, —)	117 (113,113)	127 (123, —)
110 (111, —)	187 (186, —)	127 (121, —)	187 (186,186)
131 (124,125)		149 (151,152)	
176 (175,175)		170 (—, —)	
197 (191,200)		202 (198, —)	
BaBr_2 $Pnma$			
44 (47,47)	49 (50, —)	69 (74, —)	45 (—, —)
62 (62,62)	76 (84, —)	86 (85, —)	84 (88, —)
78 (75,75)	126 (126, —)	99 (—, —)	125 (114,125)
92 (85,85)		108 (—, —)	
118 (115,113)		116 (125, —)	
137 (134,133)		133 (135, —)	
BaI_2 $Pnma$			
38 (—)	46 (—)	55 (—)	41 (—)
50 (—)	59 (—)	69 (—)	70 (—)
61 (—)	104 (—)	74 (—)	102 (—)
71 (—)		86 (—)	
94 (—)		99 (—)	
119 (—)		116 (—)	

phonon frequencies of isostructural barium halides to be in a range inversely proportional to the square root of the reduced mass of the Ba and the halide atom. For BaCl_2 and BaBr_2 , the corresponding quotient is 0.57. In fact, the calculated quotient of the highest Raman mode frequency for orthorhombic symmetry is 0.67 (see Table II and Fig. 2), and the quotient for the hexagonal equivalent is 0.72 (see Table III and Fig. 3). The inverse square root of the quotient of the reduced masses for BaI_2 and BaBr_2 is 0.87. The calculated quotient of the highest Raman mode frequency is 0.87 for the orthorhombic symmetry and 0.83 for the hexagonal symmetry.

In the evaluated Raman spectra of the barium halides in orthorhombic symmetry (top part of Figs. 2–4), all six A_g modes appear clearly. The B_{3g} mode between the fifth and sixth A_g mode also has a strong Raman intensity and can be identified in the experimental spectra of the barium halide nanocrystals provided by Pfau *et al.*⁶ despite a higher linewidth of the measured Raman peaks. Seventeen Raman modes were resolved in Ref. 7 for the bulk BaCl_2 crystal. From the theoretical results it can be concluded that the missing B_{2g} mode [theoretically predicted to have a frequency of 170 cm^{-1} (see Table II)] is the fifth B_{2g} mode and was not found because of its small Raman intensity and its vicinity to the fifth A_g mode at 176 cm^{-1} (see top part of Fig. 2 and Table II). After the reassignment of the B -type mode frequencies for BaBr_2 given in Ref. 8, the calculated Raman spectrum does not fully correspond to the mode ordering found experimentally. It was checked that the ordering of the

TABLE III. Calculated wave numbers (values in cm^{-1}) of the Raman-active zone-center phonon modes in hexagonal $P\bar{6}2m$ BaCl_2 , BaBr_2 , and BaI_2 and the assignment to their symmetry-adapted types. For comparison the modes found by Pfau *et al.*⁶ (as they could be identified) are given in parentheses for BaCl_2 and BaBr_2 . Raman measurements were not available for BaI_2 .

A'_1	E'	E''
BaCl_2 $P\bar{6}2m$		
124 (123)	88 (90)	120 (—)
224 (224)	95 (—)	154 (148)
	108 (113)	
	132 (—)	
	184 (182)	
	198 (—)	
BaBr_2 $P\bar{6}2m$		
81 (78)	61 (64)	77 (78)
143 (—)	75 (—)	98 (96)
	90 (—)	
	95 (—)	
	130 (130)	
	137 (—)	
BaI_2 $P\bar{6}2m$		
64 (—)	49 (—)	61 (—)
111 (—)	64 (—)	78 (—)
	74 (—)	
	88 (—)	
	108 (—)	
	114 (—)	

modes does not change when calculated for lattice parameters closer to the experimental ones. Therefore the discrepancies are attributed to experimental ambiguities.

The Raman spectra of the barium halides in hexagonal symmetry show more qualitative similarity because of smaller structural deviations. For the three barium halides, most intense peaks originate from the zone-center phonons assigned to A'_1 (close to and superimposing E''_1), E''_2 , and E''_5 . These three peaks can be identified from the nanocrystal measurements⁶ for BaCl_2 and BaBr_2 .

For completeness, the calculated optical properties of the barium halides in orthorhombic and hexagonal symmetry are given here. The electronic dielectric tensors ϵ_∞ are listed in Table IV. For all orthorhombic modifications, the three nonvanishing tensor components vary very little (less than 1%). The variation is somewhat larger (about 3%) for the hexagonal halides, with $\epsilon_{33} < \epsilon_{11}$ (whereas for the orthorhombic modifications, ϵ_{33} is the largest component).

Because of its centrosymmetry the orthorhombic phases of the investigated barium halides have no nonlinear optical susceptibilities of even order. For the noncentrosymmetric hexagonal BaCl_2 , BaBr_2 , and BaI_2 crystals the susceptibility tensors of second order have the form

$$d_{ij} = \begin{pmatrix} d_{\text{eff}} & -d_{\text{eff}} & 0 & 0 & 0 & 0 \\ 0 & 0 & 0 & 0 & 0 & -d_{\text{eff}} \\ 0 & 0 & 0 & 0 & 0 & 0 \end{pmatrix}, \quad (3)$$

TABLE IV. Elements of the electronic dielectric tensor ϵ_∞ for the barium halides in orthorhombic and hexagonal symmetry, calculated with parameters from Table I.

$Pnma$	BaCl_2	BaBr_2	BaI_2
ϵ_{11}	3.47	3.95	4.72
ϵ_{22}	3.49	3.93	4.73
ϵ_{33}	3.51	3.98	4.76
$P\bar{6}2m$	BaCl_2	BaBr_2	BaI_2
$\epsilon_{11} = \epsilon_{22}$	3.46	4.06	4.87
ϵ_{33}	3.36	3.94	4.70

with values $d_{\text{eff}} = d_{11}$ of 0.88 pm/V for BaCl_2 , 1.08 pm/V for BaBr_2 , and 1.40 pm/V for BaI_2 . For comparison, quartz has a d_{11} of $\simeq 0.3$ pm/V.^{31,32}

IV. CONCLUSIONS

The Raman spectra of bulk crystalline barium halides BaCl_2 , BaBr_2 , and BaI_2 in orthorhombic and hexagonal symmetry were studied with *ab initio* methods of DFT. The precision of the used methods is sufficient for the prediction and assignment of vibrational modes, as was shown by comparison with measured results from previous publications.^{6–8}

The Raman spectrum of the barium halides in orthorhombic symmetry is dominated by peaks coming from all six A_g symmetry modes and the third B_{3g} mode between the fifth and sixth A_g mode. The hexagonal ones reveal strong peaks originating from the E'_1 , $A'_{1,1}$ (close to the E'_1), E''_2 , and E'_5 modes. For both symmetries, the named peaks can be identified in nanocrystal measurements in Ref. 6

A B_{2g} vibration mode of the orthorhombic phase of BaCl_2 that was not observed in measurements (see Ref. 7) was predicted to have a frequency of 170 cm^{-1} . It is suspected that the mode was not found because of its vicinity to the A_{g5} mode with higher Raman intensity.

After adapting the symmetry type of the B -type modes of orthorhombic BaBr_2 , given in Ref. 8 for $Pbnm$ symmetry, to the $Pnma$ symmetry used here, it was found that a reassignment of these modes is necessary since not all of the observed modes could be assigned to calculated ones. This is most likely due to experimental ambiguities such as, e.g., misinterpretation because of spillover effects.

For a variety of crystals, e.g., in a powder spectrum or nanocrystals in a matrix, no identification of the vibrational modes in the Raman spectrum is possible by experimental means. A single exception is the fully symmetric A mode characterized by disappearing depolarization rates. Here, it is shown that by theoretical mode prediction the measured modes can be assigned to their symmetry types, even for broader Raman peaks as they occur for nanocrystals.

ACKNOWLEDGMENTS

The authors would like to thank the Federal Ministry for Education and Research (“Bundesministerium für Bildung und

Forschung”) for their financial support within the Centre for Innovation Competence SiLi-nano[®] (Project No. 03Z2HN11). In addition, this work was supported by the FhG Internal Programs under Grant No. Attract 692 034. The numerical

work was partially performed at the Computer Centre of the Martin Luther University of Halle-Wittenberg. We are grateful to the ABINIT group for making their code publicly available. We also thank Ulrich Skrzypczak for helpful discussions.

*Corresponding author: christian.bohley@physik.uni-halle.de

¹J. A. Johnson, S. Schweizer, B. Henke, G. Chen, J. Woodford, P. J. Newman, and D. R. MacFarlane, *J. Appl. Phys.* **100**, 033102 (2006).

²J. A. Johnson, S. Schweizer, and A. R. Lubinsky, *J. Am. Ceram. Soc.* **90**, 693 (2007).

³B. Ahrens, P. Löper, J. C. Goldschmidt, S. Glunz, B. Henke, P.-T. Miclea, and S. Schweizer, *Phys. Status Solidi A* **205**, 2822 (2008).

⁴S. Schweizer, B. Henke, B. Ahrens, C. Paßlick, P.-T. Miclea, J. Wenzel, E. Reisacher, W. Pfeiffer, and J. A. Johnson, *Proc. SPIE* **7725**, 77250X (2010).

⁵S. Aasland, M.-A. Einarsrud, and T. Grande, *J. Phys. Chem.* **100**, 5457 (1996).

⁶C. Pfau, P.-T. Miclea, C. Bohley, and S. Schweizer, *J. App. Phys.* (accepted for publication).

⁷A. Sadoc and R. Guillo, *Compt. Rend. Acad. Sci. (France) Ser. B* **273**, 203 (1971).

⁸E. Monberg and M. Nicol, *J. Chem. Phys.* **60**, 5054 (1974).

⁹H. P. Beck, *J. Solid State Chem.* **47**, 328 (1983).

¹⁰A. Haase and G. Brauer, *Z. Anorg. Allg. Chem.* **441**, 181 (1978).

¹¹A. Dubinin, B. Winkler, K. Knorr, and V. Milman, *Eur. Phys. J. B* **39**, 27 (2004).

¹²K. Schmalzl, *Phys. Rev. B* **75**, 014306 (2007).

¹³C. Jiang, C. R. Stanek, N. A. Marks, K. E. Sickafus, and B. P. Uberuaga, *Phys. Rev. B* **79**, 132110 (2009).

¹⁴Use the three-dimensional free-viewing method, which is called the cross-eyed or cross-viewing method. Aim the eyes so that the lines of sight of the eyes cross in front of the image.

¹⁵X. Gonze, G.-M. Rignanese, M. J. Verstraete, J.-M. Beuken, Y. Pouillon, R. Caracas, F. Jollet, M. Torrent, G. Zerah, M. Mikami, Ph. Ghosez, M. Veithen, J.-Y. Raty, V. Olevano, F. Bruneval, L. Reining, R. Godby, G. Onida, D. R. Hamann, and D. C. Allan, *Z. Kristallogr.* **220**, 558 (2005).

¹⁶X. Gonze, B. Amadon, P.-M. Anglade, J.-M. Beuken, F. Bottin, P. Boulanger, F. Bruneval, D. Caliste, R. Caracas, T. M. Cote, T. Deutsch, L. Genovese, P. Ghosez, M. Giantomassi, S. Goedecker, D. R. Hamann, P. Hermet, F. Jollet, G. Jomard, S. Leroux, M. Mancini, S. Mazevet, M. J. T. Oliveira, G. Onida, Y. Pouillon, T. Rangel, G.-M. Rignanese, D. Sangalli, R. Shaltaf, M. Torrent, M. J. Verstraete, G. Zerah, and J. W. Zwanziger, *Comput. Phys. Commun.* **180**, 2582 (2009).

¹⁷M. Teter, *Phys. Rev. B* **48**, 5031 (1993).

¹⁸N. Troullier and J. L. Martins, *Phys. Rev. B* **43**, 1993 (1991).

¹⁹H. J. Monkhorst and J. D. Pack, *Phys. Rev. B* **13**, 5188 (1976).

²⁰G. Liu and H. A. Eick, *J. Less-Common Met.* **149**, 47 (1989).

²¹E. B. Brackett, T. E. Brackett, and R. L. Sass, *J. Phys. Chem.* **67**, 2132 (1963).

²²M. Veithen, X. Gonze, and Ph. Ghosez, *Phys. Rev. B* **71**, 125107 (2005).

²³S. A. Prosandeev, U. Waghmare, I. Levin, and J. Maslar, *Phys. Rev. B* **71**, 214307 (2005).

²⁴I. D. Aggarwal and G. Lu, *Fluoride Glass Fiber Optics*, 1st ed. (Academic Press, New York, 1991).

²⁵A. Edgar, J.-M. Spaeth, S. Schweizer, S. Assmann, P. J. Newman, and D. R. MacFarlane, *Appl. Phys. Lett.* **75**, 2386 (1999).

²⁶R. Loudon, *Adv. Phys.* **13**, 423 (1964).

²⁷R. Wyckoff, *Crystal Structures*, Vol. 1, 2nd ed. (Wiley Interscience, New York, 1963).

²⁸*International Tables for Crystallography: Space-Group Symmetry*, Vol. A, 3rd ed. (Kluwer Academic, Dordrecht, 1989).

²⁹A. V. Bazhenov, I. S. Smirnova, T. N. Fursova, M. Yu. Maksimuk, A. B. Kulakov, and I. K. Bdikin, *Phys. Solid State* **42**, 41 (2000).

³⁰A. G. Rolo and M. I. Vasilevskiy, *J. Raman Spectrosc.* **38**, 618 (2007).

³¹D. N. Nikogosyan, *Nonlinear Optical Crystals: A Complete Survey*, 1st ed. (Springer, New York, 2005).

³²M.-Z. Huang and W. Y. Ching, *Ferroelectrics* **156**, 105 (1994).